Isı Bilimi ve Tekniği Dergisi, 32, 1, 91-99, 2012
J. of Thermal Science and Technology

ISSN 1300-3615

FORMATION OF CO-AXIAL JETS AND THEIR DOWNSTREAM DEVELOPMENT

Nevin ÇELİK*, Daniel W. BETTENHAUSENand Ryan D. LOVIK****
*University of Firat, Department of Mechatronic Engineering,
Elazig, 23279, Turkey, nevincelik23@gmail.com
**University of Minnesota, Department of Mechanical Engineering,
Minneapolis, MN 55455, USA bett0099@umn.edu and lovi0020@umn.edu

(Geliş Tarihi: 01. 11. 2010, Kabul Tarihi: 07. 01. 2011)

Abstract: A comprehensive numerical simulation has been performed to inter-relate the fluid mechanics of the formation of co-axial jets and their development downstream of the plane of jet emergence. The fluid flow was modeled as being turbulent, with corresponding Reynolds numbers in the jet-formation section of 10000, 20000, and 50000. The model was based on a fully developed pipe flow encountering a double-pipe arrangement and splitting between the two pipes. Subsequent to flow development in the central pipe and in its enveloping annulus, the flow exited into a large free space and became a co-axial free jet. The simulations were performed for geometric parameters which varied the relative cross sections of the central pipe and of the annulus and also varied the length of the jet-formation section. The overall pressure drop responsible for both the jet formation and for the subsequent free-jet development was found to be due to friction in contradistinction to inertial losses. At the jet exit, the velocity profile is discontinuous because of the intrusive presence of the walls of the pipes which bound the jet-formation section. These intrusions cause a double-humped velocity profile which disappeared with decreasing downstream distance from the jet origin. At sufficient downstream distances, the width of the jet was found to be independent of both the geometrical parameters and the Reynolds number.
Keywords: Co-axial jet, Jet formation, Numerical simulation, Turbulent jet flow, Jet spreading, CFX.

EŞ-EKSENLİ JETLERİN OLUŞUMU VE AKIMLARININ GELİŞİMİ

Özet: Eş-eksenli bir jetin oluşumu ve düzlem jet şeklinde yayılımının akışkan mekaniği ile ilgisini ortaya çıkarmak için detaylı bir sayısal çalışma hazırlanmıştır. Akışkan akışı türbülanslı ve Reynolds sayısı jet oluşum bölgesinde 10000, 20000 ve 50000 olacak şekilde modellenmiştir. Model, iç içe iki borudan oluşmuş bir boru düzeneğinin hem iç hem dış borusundan tam gelişmiş akım geçmesi temeline dayandırılmıştır. Modellemede değişken geometrik parametreler, içteki merkezi borunun kesit alanının ve jetin oluştuğu boru uzunluğunun değiştirilmesi şeklindedir. Hem jet oluşumu hem de serbest jet gelişimi nedeniyle ortaya çıkan ortalama basınç düşüşünün sürtünmeden kaynaklandığı görülmüştür. Jet çıkışında, hız profili boru cidarlarının mevcudiyetinden dolayı süreksizdir. Bu mevcudiyet aynı zamanda jet merkezinden uzaklaştıkça yavaşça kaybolan çift-yükseltili hız profillerine sebep olur. Jetten yeterince uzak mesafede jetin genişliği hem geometrik parametrelerden hem de Reynolds sayısından bağımsız hale gelmiştir.
Anahtar Kelimeler: Eş-eksenli jet, Jet oluşumu, Sayısal analiz, Türbülanslı jet akışı, Jet yayılımı, CFX.

INTRODUCTION

Although the fluid mechanics of co-axial jets has been studied by several researchers, the process of jet formation has not yet been investigated. It is reasonable to expect that the nature of the fluid motions in the jet will be affected by the flow conditions at the jet origin. In turn, the flow conditions at the jet origin are determined by the upstream fluid mechanics. It is the goal of the present paper to study the fluid flow both upstream of the jet origin and in the jet proper.

Co-axial jets are encountered in numerous industrial applications including combustion chambers of rocket engines, jet pumps, mixing tanks, cooling systems, etc. The literature review is necessarily limited to papers dealing with the fluid mechanics of the jets proper, reflecting the absence of jet-formation studies.

A review of the literature showed that the first study of co-axial jet fluid mechanics is that of Forstall and Shapiro (1951). These authors were primarily concerned with the jet-mixing problem. In this study, it was shown that the ratio of the mean velocities in the central jet to that in the annulus jet at the jet origin was the most important independent variable in determining the flow configuration and velocity profiles. Durao and Whitelaw (1973) performed experiments to explore the development of the interacting jets in the region downstream of the jet origin. In contrast, Champagne and Wygnanski (1971) investigated the velocity profiles in the fully developed jet region.

From the mean velocity and turbulence intensity experiments of Ko and his co-workers (1978, 1979 and 1978) was observed that the coaxial jet flow could be separated into: (i) initial, (ii) intermediate, and (iii) fully merged zones. The length of these zones may vary with respect to jet configurations and velocity ratios. Warda et al. (199) investigated two limiting cases of coaxial jets; round central jet ($d/D \rightarrow \infty$) and annular jet ($d/D \rightarrow 0$). The axial and radial variations of the mean and fluctuating longitudinal velocities were presented.

With regard to numerical simulations, Reynier and Ha Minh (1998) simulated compressible, turbulent coaxial jets having a large velocity ratio (inner/outer) by making use of the standard κ-ε model. The results showed a strong instability of the flow just downstream of the jet origin. In a different study, the turbulent heat transfer between the co-axial jets was modeled numerically by Kriaa et al. (2008) who focused attention on a comparison between the κ-ε and Reynolds Stress Model. Nikjooy et al. (1989) also simulated the turbulent heat transfer problem by making use of the κ-ε model.

Some of the most recent numerical researches about co-axial jets are as follow; the effects of inflow pulsation on the flow characteristics and mixing properties of turbulent confined coaxial jet flows have been studied by Jang and Sung (2010). Large eddy simulation study of mixing and intermittency of a coaxial turbulent jet discharging into an unconfined domain has been conducted by Ranga Dinesh et al. (2010). Effects of different mean velocity ratios on dynamics characteristics of a coaxial jet were analyzed by Mergheni et al. (2008).

In the present study, the dual problems of co-axial jet formation and of emergent jet development are solved numerically. A wide range of geometric and fluid flow parameters is considered. The flow will be modeled with the aid of the Shear Stress Transport (SST) turbulence model. The authors have used this model for several axisymmetric pipe-flow configurations. In addition these, same configurations were also solved using the standard κ-ε model. Comparisons of mean velocities and friction factors results obtained from the two models clearly identified those from the SST model to be in better accord with experimental data. Results will be presented for both the jet formation section and the downstream jet development.

NUMERICAL MODELLING

The co-axial jets are generated by means of two co-axial cylindrical pipes configured in a concentric orientation. The detailed information about the jet structure is illustrated in Figure 1(a), and the details of geometric configuration are exhibited in Figure 1(b) and Table 1. As seen there, the jet development section consists of a long upstream velocity development section which delivers a fully developed turbulent flow to a co-axial pipe configuration. The flow splits between the center pipe and the annular space. Both of these flows experience hydrodynamic development before exiting into a large downstream space, where they become a co-axial jet. For the numerical simulation, the flow is regarded as incompressible air flow (Mach number for the highest flow rate is found to be 0.16) with constant fluid properties. Additionally, there is no heat transfer, so isothermal conditions prevail. Axisymmetry is preserved throughout the entire flow field. The numerical solutions were performed by means of ANSYS-CFX Computational Fluid Dynamics software.

Table 1. Information of the analyzed cases.

	d_i/D_i	d_o/D_i	D_o/D_i	L/D_i
CASE I	0.55	0.7	1.14	11
CASE II	0.35	0.5	1.14	11
CASE III	0.105	0.25	1.14	11
CASE IV	0.35	0.5	1.14	25

Solution Domain and Boundary Conditions

The solution domain that was chosen for the numerical simulations is illustrated in Figure 1(b). In view of the axisymmetric nature of the problem, the portrayal of the solution domain need not display any circumferential extent. In fact, one edge of the solution domain coincides with the axis of symmetry. With respect to the letter designations of Figure 1(b), the solution domain is defined by the boundaries *abcdefghia* and *jklmj*. Along the lines *fg*, *gh*, *hi*, *jk*, *kl*, *lm*, and *mj*, the standard no-slip and impermeability conditions are applied. The line *abc* is a symmetry line, so that the radial velocity and the radial derivatives are zero there. At the upstream end of the solution domain defined by the line *ia*, the velocity profile [the universal velocity profile: $(1-r/R)^{1/6}/0.811$] is fully developed at the Reynolds number in question. For each geometrical configuration, the Reynolds number based on the total mass flowrate of the paired jets and the overall diameter of the system was varied as 10000, 20000 and 50000 ($Re = 4\dot{V}/\pi D\nu$). The turbulence intensity for the analyzed cases was chosen as 5%.

For the portion of the solution domain that encompasses the space downstream of the jet exit plane, the imposed boundary condition includes the specification of the pressure to be uniform and the velocity to be perpendicular to the surfaces *cd*, *de*, and *ef*. Since these boundaries are far removed from the zones of high fluid activity, the exact specification of the conditions thereon do not have a significant effect on the results.

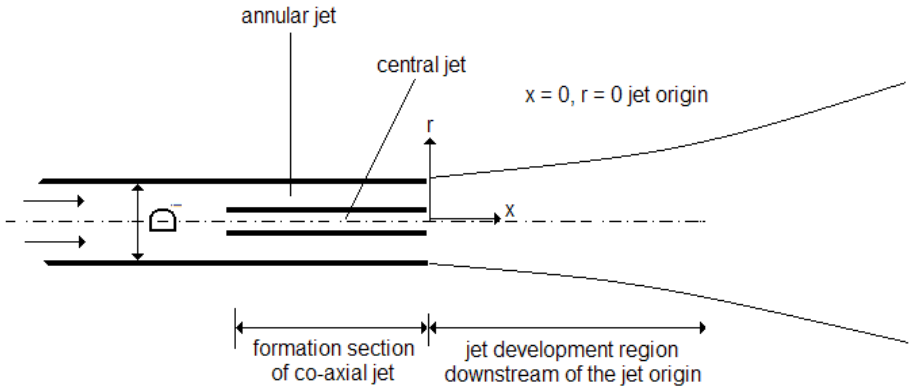

(a) Basic structure of a co-axial jet

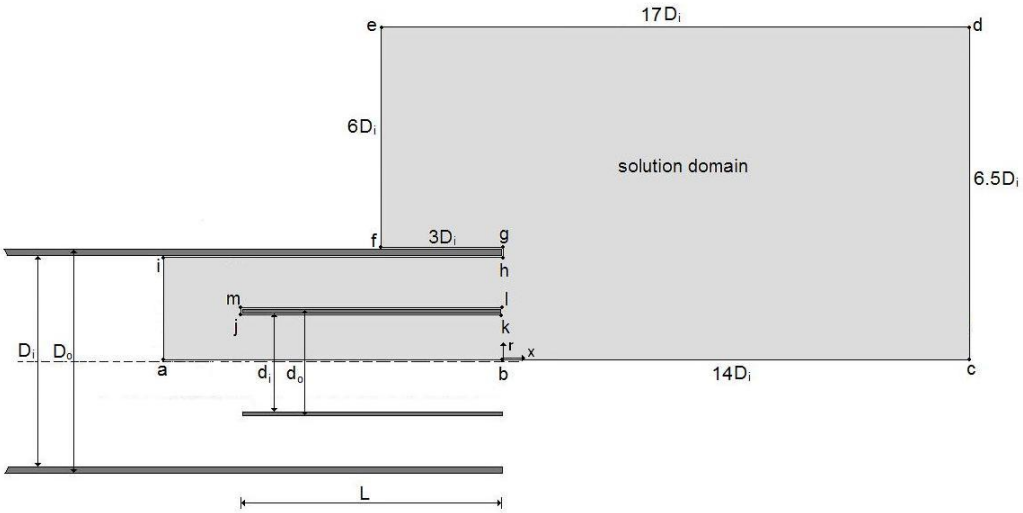

(b) Solution domain, coordinates, and dimensional nomenclature

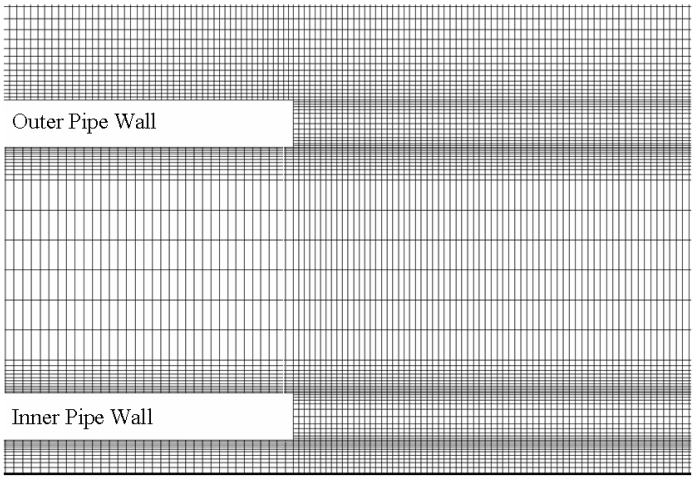

(c) Mesh structure in the neighborhood of the jet exit

Figure 1. Schematic view of the coaxial jet system.

Care was taken to extend the solution domain sufficiently far from the jet exit to avoid constraining the flow. The dimensions of the extended solution domain all referred to the inner diameter of the outer pipe D_i and are: bc = 14, cd = 6.5, de = 17, ef = 6, fg = 3. It is worthy of note that, the choice of the extended solution domain enabled interactions with the external surface of the outer pipe and sufficient space for unconstrained entrainment to occur.

Governing Equations

The governing equations encompass mass conservation, the RANS form of the Navier-Stokes equations, and the SST turbulence-model equations. They are, in Cartesian tensor form,

Mass conservation

$$\frac{\partial u_i}{\partial x_i} = 0 \qquad (1)$$

RANS equations

$$\rho\left(u_i\frac{\partial u_j}{\partial x_i}\right)=-\frac{\partial p}{\partial x_i}+\frac{\partial}{\partial x_i}\left(\left(\mu+\mu_{turb}\right)\frac{\partial u_j}{\partial x_i}\right) \quad (2)$$

$j=1,2,3$

SST equations

$$\frac{\partial\left(\rho u_i\kappa\right)}{\partial x_i}=\gamma\cdot P_\kappa-\beta_1\rho\kappa\omega+\frac{\partial}{\partial x_i}\left[\left(\mu+\frac{\mu_{turb}}{\sigma_\kappa}\right)\frac{\partial\kappa}{\partial x_i}\right] \quad (3)$$

$$\frac{\partial\left(\rho u_i\omega\right)}{\partial x_i}=A\rho S^2-\beta_2\rho\omega^2+\frac{\partial}{\partial x_i}\left[\left(\mu+\frac{\mu_{turb}}{\sigma_\omega}\right)\frac{\partial\omega}{\partial x_i}\right] \quad (4)$$
$$+2\left(1-F_1\right)\rho\frac{1}{\sigma_{\omega2}\omega}\frac{\partial\kappa}{\partial x_i}\frac{\partial\omega}{\partial x_i}$$

In Eq. (2), the quantity μ_{turb} is readily identified as the turbulent viscosity.

In the SST equations, ω i s the specific rate of turbulence destruction, P_κ is the rate of production of the turbulent kinetic energy κ, and the terms σ_κ, $\sigma_{\varpi1}$, $\sigma_{\omega2}$ are the Prandtl-number-like parameters for the transport κ and ω. Furthermore, F_1 is a blending function that facilitates the combination of the standard κ-ε model and the Wilcox κ-ω model. The term S is the absolute value of the shear strain rate, and the A and β terms are model constants.
The solution of Eqs. (3) and (4) yields the values of κ and ω, which are then used to evaluate the turbulent viscosity μ_t from

$$\mu_t=\frac{a\rho\kappa}{\max\left(a\omega,SF_2\right)} \quad (5)$$

in which F_2 is a function that limits the values of the turbulent viscosity in the near-wall region, a is a constant, and S has already been defined in connection with Eq. (5). Further details of the SST model can be found in Menter, (1994).

Mesh and Solution Accuracy

Great care was taken to create a mesh which enables the attainment of solutions of high accuracy. To this end, a mesh independence study was performed. Meshes consisting of 75000, 175000, and 310000 nodes were employed. From the corresponding solutions, the overall pressure drop was extracted, and the values for the three meshes were used to extrapolate to the case of an infinite number of nodes by use of Richardson's extrapolation method (1911). From this procedure, it was estimated that the results for the mesh with 310000 nodes were accurate to 0.5%.

An illustration of a portion of the meshed solution domain is exhibited in Figure 1(c). That figure shows the deployment of the elements in the neighborhood of the jet exit. Of particular note are the walls of the pipes that bound the formation section of the solution domain. The distribution of the elements took account of the regions of high velocity gradients by increasing the mesh density in these areas.

Selecting Suitable Turbulence Model

The selected turbulence model is the Shear Stress Transport (SST) algorithm of Menter (1994). The SST turbulence models combine the advantages of the κ–ε and κ-ω models, with a blending function that activates the κ–ε model in the core region of the flow, and shifts to the κ–ω model for the near-wall region treatment. This model has been used for the simulation of flow situations. The present authors have had broad experience with the use of the SST model and have found it to be capable of providing predictions that agree well with experimental data.

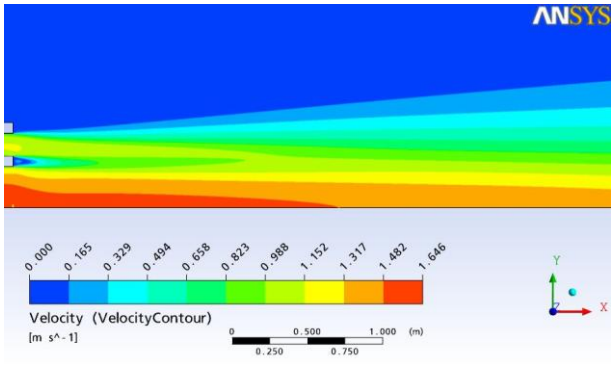

(a) κ-ε model

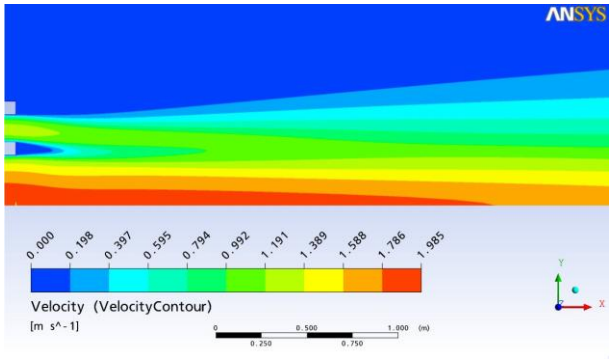

(b) SST model

Figure 2. Comparison of the turbulence models by means of velocity contours.

In this project, in order to decide the model type, some pre-analysis have been performed. In Figure 2, two contour plots are presented to show the mean velocity distribution of the co-axial free jet. Figure 2(a) exhibits the result of the κ- ε model, and Figure 2(b) shows the results for SST model. Both simulations are performed under the same conditions except for the model type. As seen from the contours, the velocity at the jet exit and at far away from the exit are quite higher in SST model than that of κ- ε model.

RESULTS AND DISCUSSIONS

Verification of Results

As a preliminary to the evaluation of the numerical results, some experimental tests were performed. In the experimental section, centerline velocities (u/U) of single circular jet ($d_i/D_i = 0$) at a certain value of Re was obtained. For this purpose, a pre-conducted experimental setup of the first author of present study was used. The detailed information about the set up has already been presented in Celik and Eren (2009 and 2010).

The axial velocity distribution of the single circular jet ($d_i/D_i = 0$) from the numerical analysis and aforementioned experiments were compared to those obtained by Lee et al. (2004) and to an earliest work in this research field, Donaldson et al. (1971). The comparison is presented in Figure 3. The experimental centerline velocity profile has an agreeable curve to that of Lee et al., (2004). The average deviation between both results is 3%. The deviation between the results of experimental work and those of Donaldson et al.'s (1971) is 9%. Additionally, the deviations between the results of present numerical work to the results of experimental work, Lee et al. (2004) and Donaldson et al. (1971) are respectively 9, 11 and 6%.

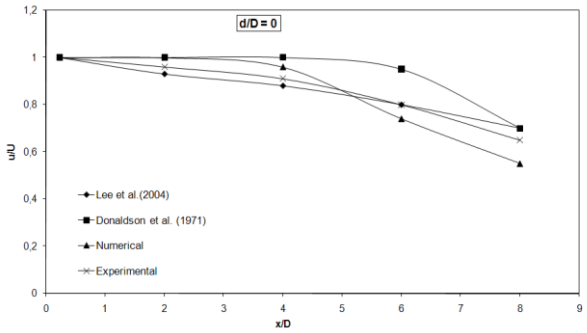

Figure 3. Comparison of the numerical centerline velocities to the experimental results.

Velocity Profiles in the Developing Jet

Attention is now focused on the development of the velocity field downstream of the point of emergence of the jets. This information is conveyed in Figures 4-7. The first three of these figures correspond to the formation length $L/D_i = 11$, while Figure 7 is for $L/D_i = 25$. Each subfigure represents Reynolds numbers of 10000, 20000, and 50000, respectively. Within each figure, velocity profiles are displayed for locations $x/D_i = 0$, 2, 4, 8, and 12. The coordinate x denotes the downstream distance from the jet origin, with $x = 0$ being the origin. The velocity profiles are normalized by the mean velocity U of the flow upstream of the coaxial pipes.

From an overall inspection of Figures 4(a-c), which pertain to the geometrical configuration defined by $d_i/D_i = 0.55$, it appears that the trends displayed in that figure are consistent for all of the investigated Re. Also worthy of note is the fact that for the range of x/D_i being considered, the velocity is nearly at $r/D_i = 2.5$. Since the solution domain extended to $r/D_i = 6$, the spread of the velocity field is properly accounted for. Special attention should be given to the velocity profile at the jet origin ($x/D_i = 0$). At that location, the velocity profile is discontinuous because of the intrusive presence of the walls of the pipes which bound the jet-formation section. These intrusions create a double-humped velocity profile. With increasing downstream distance from the jet origin $x/D_i < 4$, the humps disappear, so that for $x/D_i \geq 4$ the general shape of the velocity profiles is nearly as same as that for a single circular jet. Furthermore, the spreading of the jet is clearly in evidence as x/D_i increases, reflecting the entrainment of otherwise non-moving fluid at the jet boundary.

Figures 5 (a-c), correspond to the $d_i/D_i = 0.35$. If present case ($d_i/D_i = 0.35$) is compared with the previous case ($d_i/D_i = 0.55$), it will be seen that the present case represents a decrease of the cross-sectional area of the central jet at the exit. The differences between the profiles for the two d_i/D_is are mostly in evidence for the downstream distances $0 \leq x/D_i \leq 4$. In particular, the local maxima in the velocity profiles at the jet origin for the inner and outer jets are much more equal in magnitude for the present case than for the case conveyed in Figure 4. Furthermore, the impact of the discontinuity in the velocity profile at the jet origin is more pronounced at the second observation station, $x/D_i = 2$, than for the previous case. In addition, the general magnitudes of the velocities in the present case ($d_i/D_i = 0.35$), are lower in the near-jet-development region ($0 \leq x/D_i \leq 4$), than they were previously ($d_i/D_i = 0.55$). On the other hand, for the velocity profiles for $x/D_i > 4$, the velocity magnitudes for $d_i/D_i = 0.35$ and $d_i/D_i = 0.55$ are nearly same.

Results for the geometry defined by $d_i/D_i = 0.105$ are exhibited in Figures 6(a-c). This is a case in which the central jet at exit has extremely small cross section than the outer jet has. This deployment of jet cross section has a great impact on both the velocity distribution at the jet exit and on the downstream jet development. At the exit cross section, it is seen that the maximum velocity in the annular jet exceeds that of the central jet by a factor of 1.5 – 2, depending on the Reynolds number. Also, the humps in the profiles at $x/D_i = 2$ and 4 highlight the fact that the maximum velocity in the annulus continues to exceed that in the central jet. As was the case at the jet exit, the ratio of these maxima diminishes as the Reynolds number increases. In fact, the presence of the humps persists to $x/D_i \sim 6$ (not shown in the graph). However, for $x/D_i > 6$, the humps no longer appear and the profiles have an appearance that is similar to that of a single free jet. The trend of reduced velocity magnitude with decreasing d_i/D_i was found same when Figure 4 and 5 are compared. Similarly, the comparison of Figure 5 and 6 yields the same result. However, the overall width of the jet at the last station of observation, $x/D_i = 12$, appears to be unaffected by both the Reynolds number and by the jet geometry parameter d_i/D_i.

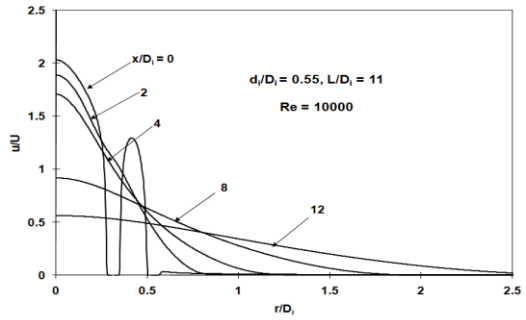

(a)

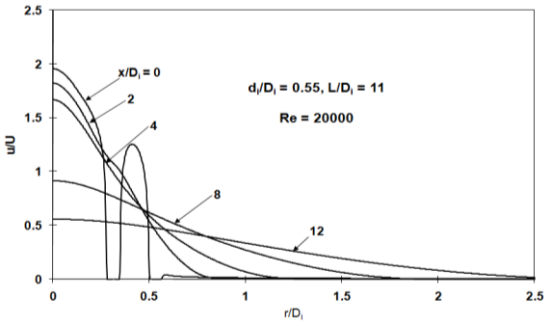

(b)

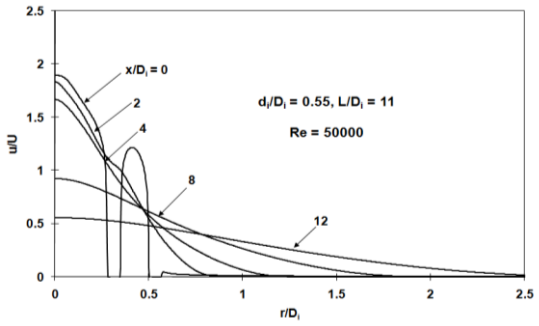

(c)

Figure 4. Radial velocity distributions for various axial distances for CASE I (d_i/D_i = 0.55, L/D_i = 11).

The effect of changing of the length of the jet formation region can be discussed by comparing the results of Figures 7(a), (b), and (c) with those of Figures 5(a), (b), and (c). These figures correspond to identical Reynolds numbers and cross-sectional geometries, but differ by the lengths of the formation sections, L/D_i = 11 and 25 for Figures 5 and 7, respectively. These figures show that the effect of the change in the formation length is mostly felt at the central jet exit and at the axial distances $0<x/D_i<4$. For all of the investigated Reynolds numbers, the velocities of the central jet are lower both at the jet exit and at x/D_i = 2 and 4 for the case of the longer formation section. This deficit is, of course, compensated by an increase in the velocities outside of the central region, but those increases are hardly detectable because the cross-sectional areas are greatly enlarged with increasing radial position. At larger downstream distances, x/D_i = 8 and 12, the effect of the longer formation length is hardly detectable. Furthermore, the extent of the jet width at x/D_i = 12 remains at a value of r/D_i = 2.5.

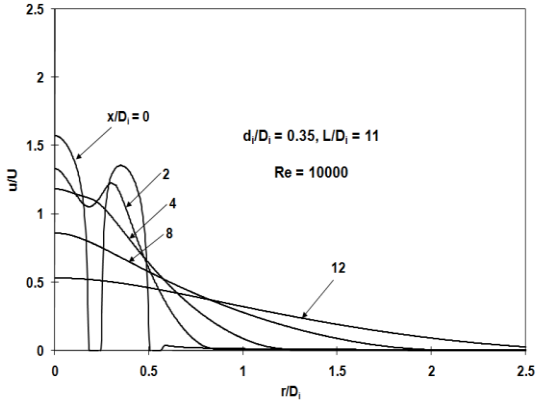

(a)

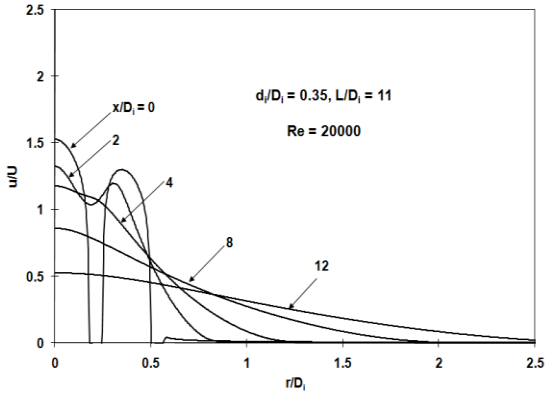

(b)

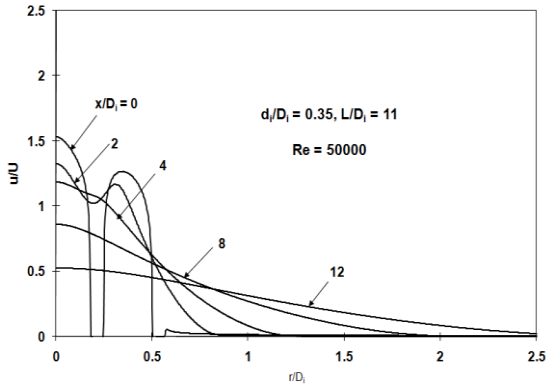

(c)

Figure 5. Radial velocity distributions for various axial distances for CASE II (d_i/D_i = 0.35, L/D_i = 11).

Overall Pressure Drop

The lengthwise pressure drop extending across the entire solution domain is presented in Figure 8. In terms of the geometry of the problem, the presented pressure drop extends from cross section *ai* to the cross section *cd*. This pressure drop accounts for the phenomena occurring both in the formation section of the coaxial jet as well as in the jet development region downstream of the jet origin. To achieve a dimensionless presentation, the pressure drop is normalized by the velocity head of the flow upstream of

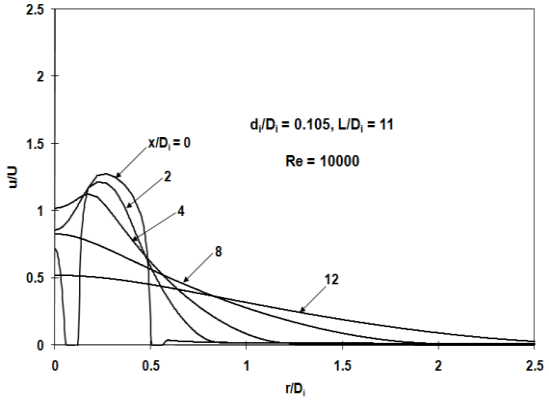

(a)

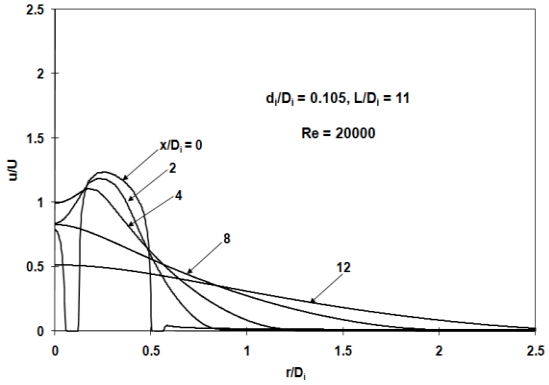

(b)

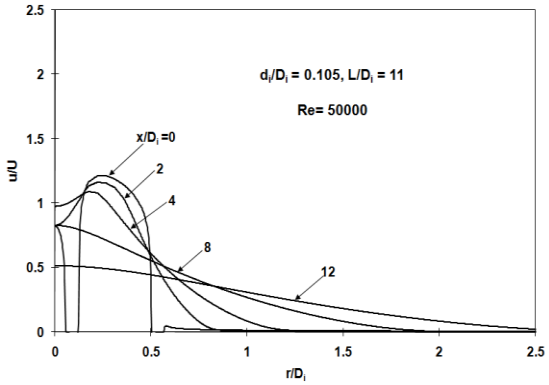

(c)

Figure 6. Radial velocity distributions for various axial distances for CASE III (d_i/D_i = 0.105, L/D_i = 11).

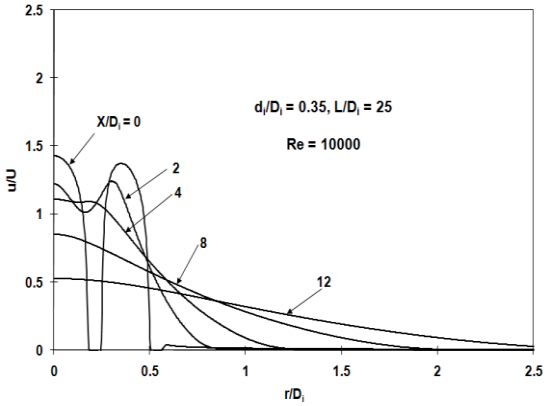

(a)

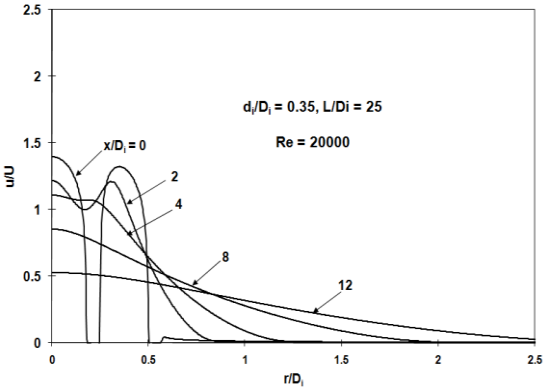

(b)

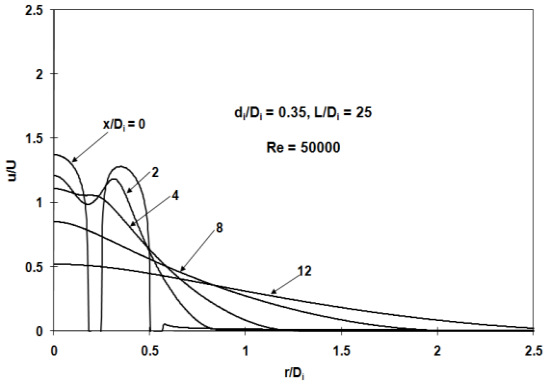

(c)

Figure 7. Radial velocity distributions for various axial distances for CASE IV (d_i/D_i = 0.35, L/D_i = 25).

the origin of the inner pipe. In particular, the velocity U is the mean velocity of the flow in the upstream region.

The figure contains results for four cases, three of which correspond to a jet development length L/D_i = 11 and the other of which is for a development length L/D_i = 25. The main focus of the work was on the length L/D_i = 11, the other length L/D_i = 25 was used to provide the direction of trends. For L/D_i = 11, the geometry of the coaxial jet system was varied according to the parameter d_i/D_i. Inspection of Figure 8 shows that the dimensionless overall pressure drop diminishes with increasing Reynolds number. This means that pressure drop is not caused because of Reynolds increment but because of friction.

Another trend that can be observed in Figure 8 is the increase in the pressure drop as the cross-sectional area of the central pipe increases relative to the cross-sectional area of the annulus. This change in the distribution of cross-sectional areas is reflected in the increasing values of d_i/D_i. This increase of pressure drop can be attributed to the substantially greater velocity gradients adjacent to the bounding wall of the pipe flow that accompany the increased cross-sectional area of that flow. Also in evidence in Figure 8 is the effect of the elongation of the formation length, expressed by the increase of L/D_i from 11 to 25. Not unexpectedly, the

pressure drop is increased by the elongation because friction is able to act over a greater length.

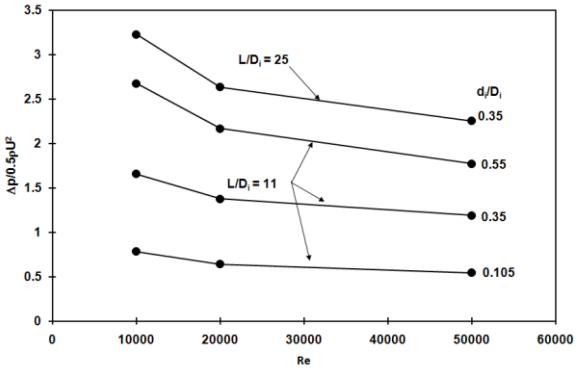

Figure 8. Pressure losses versus Reynolds number along the formation section of the coaxial pipe.

CONCLUDING REMARKS

The investigation reported here has, seemingly for the first time, analyzed both the process of jet formation and the subsequent development of the free jet. The focus of the work has been on co-axial jets which consist of a concentric arrangement of a round jet around which is wrapped a concentric-annular jet. The work is performed as a numerical simulation. The varied parameters include both geometry (diameter ratio) and flow variations (Reynolds number). Specifically, the relative cross-sectional areas of the central pipe and the surrounding annulus were varied parametrically. Another geometrical parameter was the length of the jet formation section. The results have been presented in dimensionless form.

As a conclusion; the pressure drop due to both the formation section and to the subsequent jet development was found to be dominated by friction rather than by inertial losses. The magnitude of the overall pressure loss increased as the cross-sectional area of the central pipe increased relative to the cross-sectional area of the annulus. Increases in the length of the formation section also increased the dimensionless pressure loss, as expected.

At the jet origin, the velocity profile is discontinuous because of the intrusive presence of the walls of the pipes which bound the jet-formation section. These intrusions cause a double-humped velocity profile. With increasing downstream distance from the jet origin, the humps disappear. The disappearance of the humps depends on the relative cross-sectional areas of the pipes which create the respective jet; the smaller the relative size of the central jet at exit, the longer do the humps persist. For the smallest of the central jets considered here, the disappearance of the humps was achieved at approximately six inner diameters of the outer pipe.

Elongation of the jet-formation length accentuated the size of the humps. The jet development was investigated up to a distance of 12 diameters from the jet origin. Remarkably, at that distance, the spreading of the jet was more or less independent of both of the investigated geometrical parameters and of the Reynolds number.

ACKNOWLEDGEMENT

We would like to express our gratitude to **TUBITAK** (The Scientific and Technological Research Council of Turkey) for supplying financial funding to **Nevin ÇELİK** to do Post-Doctoral Research at University of Minnesota. Also, we thank our advisor **Professor E.M. SPARROW** for his contributions to this investigation.

NOMENCLATURE

F_1, F_2	blending functions in SST model
D	diameter of the outer pipe
d	diameter of the inner pipe
L	length of the inner pipe
P	rate of production of the turbulent kinetic energy
p	pressure
r	radial distance from the axis of the jets
S	absolute value of the shear strain rate
u	streamwise velocity component
U	cross-sectional mean velocity upstream of coaxial jet formation section
u_i	velocity component
x	axial distance measured downstream of jet exit

Greek letters

α, β_1, β_2	SST model constants
ω	specific rate of turbulence destruction
μ	dynamic viscosity
κ	turbulence kinetic energy
σ	Prandtl-number-like diffusivities
ρ	density

Subscripts

i	inner
i,j	tensor notation subscripts
o	outer
$turb$	turbulent

REFERENCES

Celik, N., Eren H., Heat transfer due to impinging co-axial jets and the jets' fluid flow characteristics, *Experimental Thermal and Fluid Science*, 33, 715–727, 2009.

Celik N., Eren H., Effects of Stagnation Region Turbulence of an Impinging Jet on Heat Transfer, *Journal of Thermal Science and Technology*, 30(1), 91-98, 2010.

Champagne, F.H., Wygnanski, I.J., An experimental investigation of coaxial turbulent jets, *Int. J. Heat Mass Transfer*, 14, 1445-1464, 1971.

Chan, W.T., Ko, N.W.M., Coherent structures in the outer mixing region of annular jets, *J. Fluid Mechanics*, 89, 515-533, 1978.

Donaldson, C.D., Snedeker, R.S., Margolis, D.P., A study of free jet impingement, Part 2. Free jet turbulent structure and impingement heat transfer, *Journal of Fluid Mechanics*, 45, 477-512, 1971.

Durao, J.H., Whitelaw, J.H., Turbulent mixing in the developing region of co-axial jets, *Trans. of ASME, J. Fluids Eng.*, 95, 467-473, 1973.

Forstall, W., Shapiro, A.H., Momentum and mass transfer in co-axial gas jets, *Trans. of ASME, J. Applied Mechanics*, 18, 219-228, 1951.

Jang, S.J., Sung, H.J., Effects of inflow pulsation on a turbulent coaxial jet, *Int. J. Heat and Fluid Flow*, 31(3), 351-367, 2010.

Ko, N.W.M., Chan, W.T., Similarity in the initial region of annular jets: three configurations, *J. Fluid Mechanics*, 84, 641-656, 1978.

Ko, N.W.M., Chan, W.T., The inner regions of annular jets, *J. of Fluid Mechanics*, 93, 549-584, 1979.

Kriaa, W., Abderrazak, K., Mhiri, H., Le Palec, G., Bounot, P., A numerical study of non-isothermal turbulent co-axial jets, *Heat and Mass Transfer*, 44, 1051-1063, 2008.

Lee, D.H., Song, J. Jo, M.C., The effects of nozzle diameter on impinging jet heat transfer and fluid flow, *Trans. ASME, J. Heat Transfer*, 126, 554-557, 2004.

Menter, F., Two-equation eddy-viscosity turbulence models for engineering applications, *AIAA Journal*, 32, 1598-1605, 1994.

Mergheni, M.A., Boushaki, T., Sautet, J.-C., Godard, G., Ticha, H.B., Nasrallah, S.B.: Effects of different mean velocity ratios on dynamics characteristics of a coaxial jet, *Thermal Science*, 12 (2), 49-58, 2008.

Nikjooy, M., Karki, K.C., Mongia, H.C., A numerical and experimental study of co-axial jets, *Int. J. Heat and Fluid Flow*, 10, 253-261, 1989.

Ranga-Dinesh, K.K.J., Savill, A.M., Jenkins, K.W., Kirkpatrick, M.P., A study of mixing and intermittency in a coaxial turbulent jet, *Fluid Dynamics Research*, Article no. 025507, 42 (2), 2010.

Reynier, P., Ha-Minh, H., Numerical prediction of unsteady compressible turbulent co-axial jets, *Comp. Fluids*, 27, 239-254, 1998.

Richardson, L.F., The approximate arithmetical solution by finite differences of physical problems including differential equations, with an application to the stresses in a masonry dam, *Philosophical Transactions of Royal Society of London*, Series A, 210, 307–357, 1911.

Warda, H.A., Kassab, S.Z., Elshorbagy, K.A., Elsaadawy, E.A., An experimental investigation of free turbulent round and annular jets, *Flow Measurement and Instrumentation*, 10, 1-14, 1999.